NATIONAL AERONAUTICS AND SPACE ADMINISTRATION

Technical Report No. 32-946

Comparison of Liquid-Metal Magnetohydrodynamic Power Conversion Cycles

E. Weinberg

L. G. Hays

JET PROPULSION LABORATORY

CALIFORNIA INSTITUTE OF TECHNOLOGY

PASADENA, CALIFORNIA

August 15, 1966

NATIONAL AERONAUTICS AND SPACE ADMINISTRATION

Technical Report No. 32-946

Comparison of Liquid-Metal Magnetohydrodynamic Power Conversion Cycles

E. Weinberg
L. G. Hays

D. R. Bartz, *Manager*
Research and Advanced Concepts Section

JET PROPULSION LABORATORY
CALIFORNIA INSTITUTE OF TECHNOLOGY
PASADENA, CALIFORNIA

August 15, 1966

Prepared Under Contract No. NAS 7-100
National Aeronautics & Space Administration

CONTENTS

CONTENTS (Cont'd)

TABLES

FIGURES

FIGURES (Cont'd)

ABSTRACT

Various two-phase liquid-metal magnetohydrodynamic (MHD) power conversion cycles employing either a separator or jet condenser are compared on the basis of cycle efficiency, prime radiator area, and specific weight. The cycles are investigated first from the standpoint of coalescence on a wall (of the separator or jet condenser) with attendant friction and deflection energy losses and, second, from the standpoint of liquid coalescence with no friction or deflection energy losses. The results of this study for the first condition show that (1) the two-component cycles, both separator and condenser (employing lithium and cesium), have efficiencies of 6 to 7%, while the single-component (one chemical species—cesium or potassium) have maximum efficiencies of only 3 to 4%, and (2) the two-component separator cycle (cesium-lithium) has a slightly higher efficiency and smaller radiator area than the two-component condenser cycles (cesium-lithium), if 100% liquid impingement is assumed on the condenser and separator walls. For the second condition—operation without separator and condenser friction or deflection—it was shown that (1) the two-component cycles require about half as much radiator area as the single-component cycles, for a given efficiency, and (2) the efficiency of the two-component condenser cycles (cesium-lithium) increases indefinitely with decreasing rejection temperature, while the efficiency of the two-component separator cycle (cesium-lithium) is limited to 13%. It thus appears that the most promising cycle for space applications is the two component (cesium-lithium) separator cycle, if 100% liquid impingement occurs on the walls of the jet condenser and on the separator. The two-component (cesium-lithium) condenser cycles appear promising for ultimate high efficiency, should it be possible to eliminate condenser friction.

I. INTRODUCTION

The high reliability and long lifetime required in space powerplants make systems without moving mechanical parts particularly attractive. One of the methods available for converting nuclear reactor heat to electric energy without the use of moving parts is magnetohydrodynamic (MHD) power conversion, wherein electric power is generated by forcing a conducting fluid, rather than a solid conductor, through a magnetic field. The conducting fluid may be a plasma or a liquid metal.

A number of liquid-metal MHD energy conversion cycles have been proposed for power conversion at the reactor temperatures presently attainable, 1800 to 2200°F. All of these cycles are based on the principle of accelerating a liquid metal, coalescing the liquid into a film or jet by use of either a separator or condenser, and employing the liquid metal to drive an MHD generator. Systems using this principle may employ either a two-component or one-component working fluid. By component is meant each chemical species used in the cycle.

The four power conversion cycles compared in this report, and the publications in which they were initially proposed, are:

1. Two-component separator cycle (Ref. 1)
2. Single-component separator cycle (Ref. 2)
3. Single-component jet condenser cycle (Refs. 2, 3, and 4)
4. Two-component jet condenser cycle[1]

Other types of liquid-metal MHD systems not covered by the above classifications have also appeared in the literature (Refs. 5, 6, and 7). However, the cycles discussed in Refs. 5 and 6 depend on power generation from a high void-fraction two-component mixture; the cycle of Ref. 5 depends, additionally, on condensation at high velocity with neither separation nor coolant injection losses. The cycle of Ref. 7 employs thermally driven reciprocating flow. The principles of operation for these systems are not sufficiently established for them to be considered at this time.

This report compares the four liquid MHD cycles on the bases of cycle efficiency (η), prime radiator area (A_{rad}), and specific weight (W_s). The cycles are investigated from two standpoints: (1) liquid coalescence with no friction or deflection energy losses and (2) coalescence on a wall (of the separator or jet condenser) with attendant friction and deflection energy loss. In case 1, the differences between cycles due to thermodynamic effects can be calculated; and in case 2, the additional differences due to frictional effects can be found.

The first section describes the cycles, assumptions, and equations used in the analysis. The optimization techniques and fluid properties used are then discussed. Finally, numerical results are used to compare the cycles.

[1]L. Prem, private communication.

II. CYCLE ANALYSIS

A. Two-Component Separator Cycle

The two-component separator cycle is shown schematically in Fig. 1. In this cycle, a condensable fluid, component *a*, circulates in the vapor loop, and a liquid metal, component *b*, circulates in the liquid loop. In practice, some component *b* is also present in the vapor loop because of the finite vapor pressure of component *b*, and some component *a* is present in the liquid loop because of the finite solubility of component *a* in component *b*. As shown later, the most favorable combination is cesium (Cs) as component *a* and lithium (Li) as component *b*. The process in the conversion system may then be described as follows: the Cs leaves the radiator as a condensate, is pumped by an EM pump through the regenerative heat exchanger to the nozzle, vaporizes on contact with the Li, atomizes and accelerates the Li in the nozzle, separates from the Li in the separator, and returns to the radiator through the regenerative heat exchanger, the latter removing the Cs superheat. The Li leaves the separator at high velocity (typically 500 ft/sec),

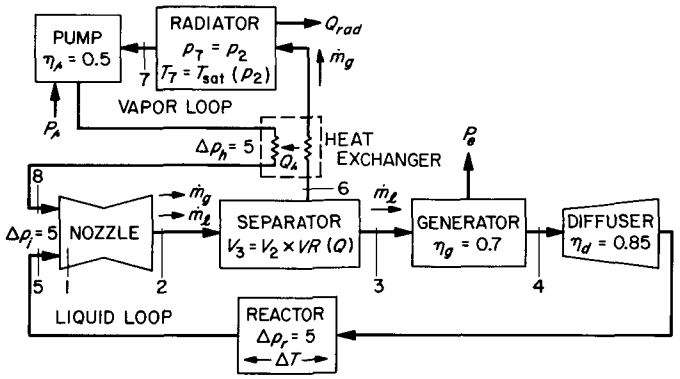

Fig. 1. Two-component separator cycle

decelerates through the production of electric power in the MHD generator, and leaves the generator with sufficient velocity (typically 300 ft/sec) to return through a diffuser to the reactor where the Li is reheated.

By *reactor* and *radiator* are merely meant the heat source and heat sink for the cycle. In practice, these components may consist of heat exchangers connected through separate loops to the actual reactor and radiator, but the cycle analysis is the same.

The key energy conversion steps in the process are:

1. Transfer of heat from the reactor to the liquid
2. Conversion of this heat to vapor enthalpy
3. Conversion of part of the vapor enthalpy to kinetic energy of the liquid
4. Conversion of most of the liquid kinetic energy to electric power in the generator, the remainder going to losses and to pressure recovery in the diffuser
5. Condensation of the vapor in the radiator

The following simplifying assumptions are made:

1. *The two-phase nozzle exit velocity is that for one-dimensional flow of spherical droplets that break up to limit the Weber Number to 6 (Refs. 8 and 9).*
2. *The separator exit velocity is calculated for the condition of flat-plate skin friction, by use of the relationship derived in Ref. 10.*
3. *The MHD generator operates at constant pressure and has an efficiency, η_g, equal to 0.7.*
4. *The temperature drop across the condensing vapor film, along the length of the radiator, and through the radiator tube wall may be neglected.*
5. *The diffuser efficiency, η_d, is equal to 0.85.*
6. *The electromagnetic (EM) pump efficiency, η_p, is equal to 0.50.*
7. *The radiator surface emissivity, ε, is equal to 0.9.*
8. *The pressure drops across the vapor side of the regenerative heat exchanger and across the reactor are 5 psi.*
9. *The injection pressure drop at the nozzle entrance is 5 psi for each loop.*
10. *The radiator exit pressure is equal to the nozzle exhaust pressure.*

The analysis of the nozzle has been verified by experiments using nitrogen-water and freon-water mixtures (Refs. 8 and 11). The analysis of separator exit velocity has been verified by use of nitrogen-water mixtures (Ref. 11). It has been concluded that an efficiency of 70% is an attainable upper limit with liquid-metal MHD generators (Refs. 12 and 13). The temperature drop across the fluid film and through the tube wall is negligible compared with the absolute temperature of the tube wall. A diffuser efficiency of 85% appears attainable, based on experimental results reported in Ref. 11. Pump efficiencies as high as 50% have been obtained by EM pumps (Ref. 14). A number of coatings are presently available with emissivities between 0.85 and 0.90 for temperatures between 800 and 1600°F. The pressure drops across the components are typical values for these devices. The pressure drop through the heat exchanger and radiator is compensated for by pressure recovery from the high velocity vapor leaving the separator.

The mass, momentum, and energy balances around each component, and the equations used to calculate cycle performance variables are presented below.

1. Two-Phase Nozzle

The nozzle exhaust conditions are calculated by a finite difference method described in Ref. 9. The method employs one-dimensional two-phase flow equations, and the Weber number = 6 droplet breakup criterion. The effects of solubility, liquid vapor pressure, and property variations are also included. The projected area of the separator is equated to the exhaust area of the nozzle for each exit velocity.

2. Separator

The loss in kinetic energy of the liquid in the separator results from deflection and skin friction. The velocity of

the liquid leaving the separator may be calculated by application of the momentum equation to the situation in which a two-phase jet impinges on a cone or an inclined plate. This analysis is described in Ref. 10. The optimum separator angle giving maximum exit velocity is employed. For cycle calculations without separator friction or deflection loss, the velocity of the liquid leaving the separator is taken equal to the nozzle exhaust velocity. This result would describe the flow if separation of liquid from vapor could be achieved by coalescing the liquid phase within the flow passage, but without striking the wall.

3. MHD Generator

The net electric power output from the cycle is the fraction, η_g, of the kinetic energy change of the liquid across the generator, minus the electric power supplied to the condensate pump. Thus,

$$P_e = \tfrac{1}{2}\eta_g \dot{m}_l (V_3^2 - V_4^2) - P_p \qquad (1)$$

where P_e is the output power, $\dot{m}_l$ is the mass flow rate of the liquid, V is the velocity, and P_p is the electric power supplied to the condensate pump.

4. Diffuser

The pressure rise across the diffuser is a fraction, η_d, of the inlet dynamic pressure. Thus,

$$p_1 - p_2 + \Delta p_r + \Delta p_i = \tfrac{1}{2}\eta_d \rho_{l_b} V_4^2 \qquad (2)$$

where ρ_{l_b} is the density of the liquid, taken as the density of component b liquid.

5. Regenerative Heat Exchanger

The regenerative heat exchanger raises the efficiency of the cycle by cooling the vapor entering the radiator, while preheating the condensate. Thus, the heat output during cooling is the sum of that for desuperheating the vapor loop component (a) and condensing the small amount of liquid loop component (b vapor) that is carried over. The heat rejected by desuperheating component a is

$$Q_a = \dot{m}_g (1 - \beta) C_{g_a} (T_2 - T_7) \qquad (3)$$

where T_6 has been replaced by T_2, a close approximation; β is the mass fraction of component b in the gas, and C_{g_a} is the heat capacity of component a in the gaseous phase.

The heat rejected in condensing and cooling component b is given by

$$Q_{b_1} = \dot{m}_g \beta L_b \qquad (4)$$

for condensing, and

$$Q_{b_2} = \dot{m}_g \beta C_{l_b} (T_2 - T_7) \qquad (5)$$

for cooling.

The total heat input available to the regenerative heat exchanger is, therefore,

$$Q_c = Q_a + Q_{b_1} + Q_{b_2}$$

$$Q_c = \dot{m}_g \Big\{ (1 - \beta) C_{g_a} (T_2 - T_7) + \beta \Big[L_b + C_{l_b} (T_2 - T_7) \Big] \Big\} \qquad (6)$$

The available cooling capacity of the condensate is the amount of heat the condensate would acquire in being heated from the radiator exit temperature to the nozzle inlet temperature (T_1) minus the added heat caused by the inefficiency of the pump. If the cooling capacity of the small amount of entrained component b is neglected, the available cooling is

$$Q_l = \dot{m}_g C_{l_a} (T_1 - T_7) - (1 - \eta_p) P_p \qquad (7)$$

The heat exchanger heat transfer, Q_h, is the smaller of Q_c and Q_l.

6. Radiator

The heat radiated to space is equal to the latent heat of the vapor of component a as it condenses at T_7, plus any superheat of component a as well as latent heat of component b not removed in the regenerative heater. Thus,

$$Q_{rad} = \dot{m}_g (1 - \beta) L_a + Q_c - Q_h \qquad (8)$$

7. EM Pump

The electric power required to pump the condensate from the exit of the radiator, through the regenerative heater, to the entrance of the nozzle is the product of

volume flow rate and pressure rise, divided by the pump efficiency,

$$P_p = \frac{\dot{m}_g (p_1 - p_2 + \Delta p_h + \Delta p_i)}{\eta_p \rho l_a} \quad (9)$$

8. Cycle Efficiency

The cycle efficiency is the output power divided by the sum of the output power and the radiated power, or

$$\eta = \frac{P_e}{P_e + Q_{\text{rad}}} \quad (10)$$

9. Prime Radiator Area

The prime radiator area is the radiating area per kw of electric output power required to radiate the waste heat, Q_{rad}, to space when the radiator temperature is everywhere equal to the fluid temperature.

The Stefan-Boltzmann law is used to calculate this area. Thus,

$$A_{\text{rad}} = \frac{Q_{\text{rad}}}{\sigma \varepsilon T_7^4 P_e} \quad (11)$$

where σ is the Stefan-Boltzmann constant.

10. Specific Weight

A simple specific weight relation is employed for comparative purposes at the 300-kwe level. The equation is

$$W_s = C_1 + \frac{C_2}{\sqrt{\eta}} + C_3 A_{\text{rad}} \quad (12)$$

The symbol C_1 represents the allowance for the weight of the power conversion system exclusive of the radiator. A weight allowance of 10 lb/kwe is used in this study. The second term represents the reactor weight, which was taken as 2800 lb for a 5-Mw reactor and assumed to be proportional to the ½ power of the thermal output in this range of power. The last term represents the radiator weight. In this study, a radiator weight of 2 lb/ft² was assumed, and the prime radiator area was increased by a factor of 1.5 to allow for the fins in an actual radiator.

These values are felt to be representative of 2000°F technology. Other numbers would certainly result from the design of a specific system. However, these weights should be sufficiently valid to show the functional dependence of specific weight on efficiency and radiator area.

B. Single-Component Separator Cycle

A liquid MHD powerplant employing a single-component working fluid, such as potassium or cesium, is shown schematically in Fig. 2. In this cycle, the condensate leaves the radiator and is pumped by an EM pump to the nozzle where it mixes with two-phase fluid from the heat source. The resulting two-phase mixture then atomizes further and is accelerated in the two-phase nozzle. The vapor is separated from the liquid metal in the separator at the nozzle exit and returned to the radiator. The liquid leaves the separator at high velocity (typically 650 ft/sec for K, 450 ft/sec for Cs), decelerates through the production of electric power in the MHD generator, and leaves the generator with sufficient velocity (typically 200 ft/sec for K, 150 ft/sec for Cs) to return through a diffuser to the reactor or boiler where the liquid metal is reheated and partially vaporized.

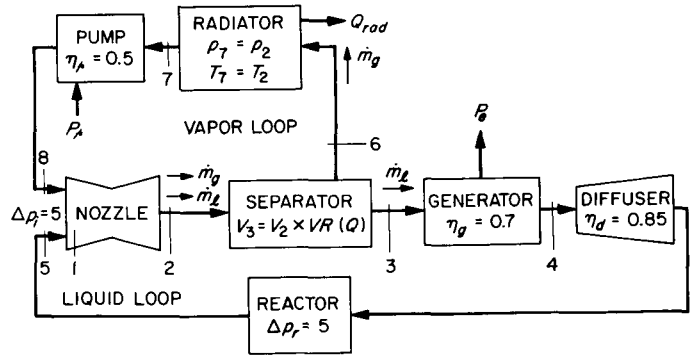

Fig. 2. Single-component separator cycle

This cycle differs from the two-component cycle in that the nozzle exit temperature in the single-component cycle is equal to the saturation temperature at p_2, and the reactor must, therefore, heat the liquid over the full temperature range of the cycle. In addition, partial vaporization of the liquid occurs directly in the reactor. Otherwise, the key energy conversion steps in this cycle and the simplifying assumptions made are identical to those for the two-component separator cycle.

The mass, momentum, and energy balances around each component, and the equations used to calculate cycle performance variables are presented below.

1. Two-Phase Nozzle

The nozzle exhaust conditions are calculated from the same two-phase nozzle equations as for the two-component case, with the additional constraint that the two phases are the same chemical species and are both at the saturation temperature corresponding to the local pressure (Ref. 9).

2. Separator

The analysis used to calculate the loss in the kinetic energy of the liquid as it travels along the separator surface is identical to the analysis used in the two-component separator cycle analysis. The expression for frictionless separation was again obtained by equating the separator exit velocity to the nozzle exhaust velocity.

3. MHD Generator

The net electric power output from this cycle, which is also given by Eq. (1), is the fraction, η_g, of the kinetic energy change of the liquid across the generator minus the electric power supplied to the condensate pump.

4. Diffuser

The pressure rise across the diffuser is the fraction, η_d, of the inlet dynamic pressure (Eq. 2).

5. Radiator

The waste heat radiated to space is the latent heat of the vapor as it condenses isothermally at $T_7 = T_2$. The radiated power is, therefore,

$$Q_{rad} = \dot{m}_g L \tag{13}$$

6. EM Pump

The electric power required to pump the condensate from the exit of the radiator to the entrance of the nozzle is the product of the volume flow rate and the pressure rise, divided by the pump efficiency, or

$$P_p = \frac{\dot{m}_g (p_1 - p_2 + \Delta p_i)}{\eta_p \rho_l} \tag{14}$$

7. Cycle Efficiency

The cycle efficiency is again the output power divided by the sum of the output power and the radiated power (Eq. 10).

8. Prime Radiator Area

The Stefan-Boltzmann law is used to calculate the area/kw of output power required to radiate the waste heat to space. Thus,

$$A_{rad} = \frac{Q_{rad}}{\sigma \varepsilon T_2^4 P_e} \tag{15}$$

9. Specific Weight

The specific weight equation is identical to Eq. (12), the one presented for the two-component separator cycle. It is, therefore, subject to the same limitations. The constants, C_1, C_2, and C_3, were assumed to have the same values.

C. Single-Component Jet Condenser Cycle

A schematic of the single-component jet condenser cycle is presented in Fig. 3, and a diagram of the jet condenser, itself, is given in Fig. 4. In this cycle, a low-quality mixture of a liquid metal and its own vapor (cesium or potassium) is expanded through a nozzle. The vapor from the nozzle exhaust is completely condensed in the jet condenser by the injection of subcooled liquid metal, referred to as the coolant. The liquid then leaves the jet condenser with a velocity that is higher than the coolant injection velocity (exit velocity typically 900 ft/sec for K, 600 ft/sec for Cs). A portion of the exit liquid flow passes through a diffuser to the radiator where it is subcooled, then reinjected into the condenser as the coolant. The other portion of the exit liquid decelerates through the production of electric power in the MHD generator, then leaves the generator with sufficient velocity (typically 200 ft/sec for K, 150 ft/sec for Cs), to return through a diffuser to the reactor, where it is partially vaporized.

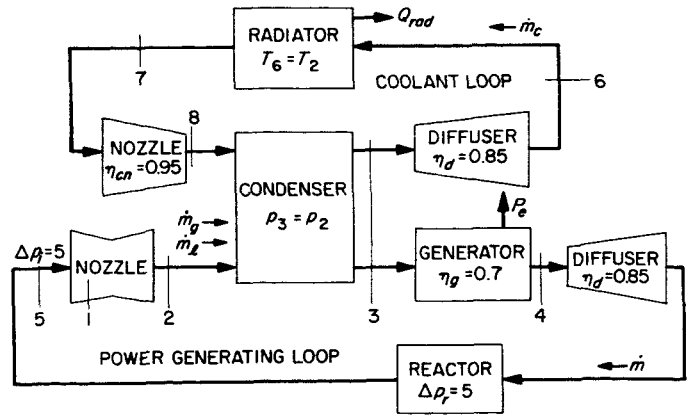

Fig. 3. Single-component jet condenser cycle

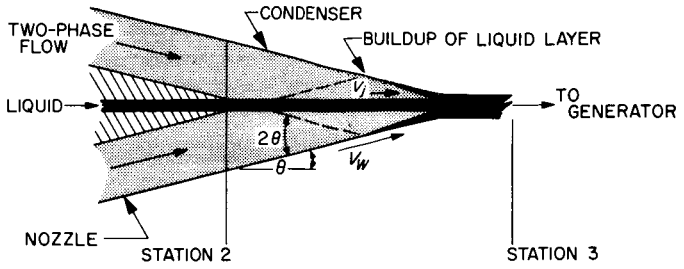

Fig. 4. Jet condenser with liquid impingement

The key energy conversion steps in the process are:

1. Transfer of heat from the reactor to the fluid, partially vaporizing the fluid and increasing its enthalpy
2. Conversion of the available enthalpy of the vapor to kinetic energy of the vapor and liquid in the two-phase nozzle
3. Condensation of the vapor and entrainment of the liquid, from the power loop nozzle, on the injected coolant liquid (Momentum is transferred in this step increasing the kinetic energy of the coolant.)
4. Conversion of most of the kinetic energy of the liquid leaving the condenser to electric power in the generator, the remainder going to losses in both loops and to pressure recovery in the diffuser of the power loop
5. Subcooling of the coolant liquid in the radiator

The following simplifying assumptions are made:

1. *The two-phase nozzle exit velocity is that for one-dimensional flow of spherical droplets that break up to limit the Weber number to 6 (Refs. 8 and 9), with the two phases being the same chemical species and both being at the saturation temperature corresponding to the local pressure.*
2. *The MHD generator operates at constant pressure and has an efficiency of 0.7.*
3. *The temperature drop across the radiator tube wall may be neglected.*
4. *The efficiency of both diffusers is 0.85.*
5. *The radiator surface emissivity is equal to 0.9.*
6. *The pressure drops across the reactor and across the injector of the two-phase nozzle are 5 psi.*
7. *The condenser operates at constant pressure (equal to nozzle exit saturation pressure).*
8. *The liquid leaving the condenser is saturated.*
9. *All of the liquid leaving the two-phase nozzle impinges on the condenser wall, and the liquid velocity is reduced by flat-plate skin friction according to the relationship derived in Ref. 10.*
10. *The effects on heat rejection and radiator temperature of losses in the coolant nozzle and coolant diffuser may be neglected.*
11. *The efficiency of the coolant nozzle is 0.95.*

Assumptions 1–6 are justified on the same basis as previously discussed for the separator cycles.

Operation of the jet condenser at constant pressure, assumption 7, was analyzed because this situation is closest to the operating conditions of units that have exhibited stable performance with high momentum transfer. Also, reasonably good agreement ($\pm 30\%$) between experimental results and performance predicted on this basis has been obtained (Refs. 15, 16, and 17). Operation with inlet pressure lower than exit pressure would enable somewhat higher theoretical cycle performance to be attained if the increased frictional losses, caused by the larger nozzle exit area, were not excessive. Preliminary calculations, however, show the frictionless constant pressure results to be only 20 to 30% less than the most ideal variable pressure case (no wall friction, local vapor pressure equal to saturation pressure of the liquid). This result, together with the uncertainties of stability and heat transfer for variable pressure operation, led to the choice of the constant pressure model for analysis.

Assumption 8, saturation at the condenser exit, is adopted because it gives minimum radiator area; subcooling at the condenser exit would lower the radiator temperature without changing the heat rejected.

Assumption 9 stems from the experimental observation (Ref. 11) that the liquid leaving a two-phase nozzle is not significantly deflected by a change in the direction of the gas phase. Instead, the liquid follows a straight path until striking a solid surface which, in this case, is the wall of the condenser. (A possibility exists for orienting the nozzle to avoid wall impingement, as discussed in Ref. 18.) In one set of calculations in this report, the friction assumption will be eliminated, and V_3 will be assumed equal to V_2. The effect of intermediate fractions of liquid impingement will also be presented.

Assumption 10 is shown in the Appendix to be a satisfactory approximation. Assumption 11 represents an attainable efficiency for liquid nozzles.

The mass, momentum, and energy balances around each component, and the equations used to calculate cycle performance variables are presented below.

1. Two-Phase Nozzle

The equations used in the analysis of the single-component separator cycle are also used in this analysis.

2. Coolant Inlet Velocity

The dynamic pressure of the coolant entering the condenser is a fraction, η_{cn}, of the pressure difference across the coolant nozzle. Thus,

$$\tfrac{1}{2}\rho_l V_8^2 = \eta_{cn}(p_7 - p_8) \tag{16}$$

Since $p_8 = p_2$,

$$p_7 - p_2 = \tfrac{1}{2}\frac{\rho_l V_8^2}{\eta_{cn}} = \tfrac{1}{2}\eta_d \rho_l V_3^2 \tag{17}$$

where the radiator pressure drop has been neglected relative to p_7.

Finally,

$$V_8 = (\eta_d \eta_{cn})^{1/2} V_3 \tag{18}$$

3. Jet Condenser

The vapor exhaust flow from the two-phase nozzle is completely condensed by the injection of subcooled liquid metal into the jet condenser. The liquid leaves with a velocity that is higher than the subcooled liquid injection velocity. The geometry chosen for analysis is that shown in Fig. 4. Since

$$T_2 = T_3 = T_{sat}(p_2)$$

the heat transferred to the coolant is given by

$$\dot{m}_g L = \dot{m}_c C_l (T_2 - T_7) \tag{19}$$

For generality, a fraction, ψ, of the two-phase nozzle flow will be assumed to collect on the coolant jet without impinging on the wall. The remainder impinges on the opposite wall at an angle 2θ, as shown in Fig. 4. With constant pressure mixing the momentum balance for the flow collecting on the coolant jet is:

$$\dot{m}_c V_8 + (\dot{m}_g + \psi\dot{m}_l) V_2 \cos\theta = (\dot{m}_g + \psi\dot{m}_l + \dot{m}_c)V_j \tag{20}$$

By substituting for V_8,

$$\dot{m}_c (\eta_d \eta_{cn})^{1/2} V_3 + (\dot{m}_g + \psi\dot{m}_l)V_2 \cos\theta = (\dot{m}_g + \psi\dot{m}_l + \dot{m}_c)V_j \tag{21}$$

The mixing of the jet with the wall flow gives the condenser exit velocity V_3.

Thus,

$$(\dot{m}_g + \psi\dot{m}_l + \dot{m}_c)V_j + (1 - \psi)\dot{m}_l V_W \cos\theta = (\dot{m}_c + \dot{m})V_3 \tag{22}$$

where $\dot{m}$ is the total nozzle flow rate $\dot{m}_g + \dot{m}_l$. Combining Eq. (21) with Eq. (22) gives

$$\dot{m}_c (\eta_d \eta_{cn})^{1/2} V_3 + (\dot{m}_g + \psi\dot{m}_l)V_2 \cos\theta = (\dot{m}_c + \dot{m})V_3 - (1 - \psi)\dot{m}_l V_W \cos\theta \tag{23}$$

The velocity of the liquid that has impinged on the wall, V_W, is found by using the analysis presented in Ref. 10, from which

$$V_W = \frac{(1-\psi)\dot{m}_l \sin 2\theta}{C_f \rho_l A_2}\left\{\left[1 + \frac{2C_f \rho_l V_2 A_2}{(1-\psi)\dot{m}_l \tan 2\theta}\right]^{1/2} - 1\right\} \tag{24}$$

where C_f is the skin friction coefficient.

The solution for V_3 is:

$$V_3 = \frac{(\dot{m}_g + \psi\dot{m}_l)V_2 \cos\theta + (1-\psi)\dot{m}_l\ V_W \cos\theta}{\dot{m} + [1 - (\eta_d\,\eta_{cn})^{1/2}]\dot{m}_c} \tag{25}$$

In accordance with assumption 9, the exit velocities for the cycle calculations with friction were obtained by setting $\psi = 0$ and employing the value of θ that maximized V_3. Optimum values of θ were found to range from 7 to 10 deg. The exit velocities for the frictionless calculations were obtained by setting $\theta = 0$ and $\psi = 1$ in Eq. (25).

4. MHD Generator

A portion of the flow leaving the condenser, $\dot{m}$, is passed through the generator. The net electric power output from the cycle is then a fraction, η_g, of the kinetic energy change of the liquid across the generator. Thus,

$$P_e = \tfrac{1}{2}\eta_g \dot{m}\ (V_3^2 - V_4^2) \tag{26}$$

5. Diffuser

The pressure rise across the diffuser is a fraction, η_d, of the inlet dynamic pressure. Thus,

$$p_1 - p_2 + \Delta p_i + \Delta p_r = \tfrac{1}{2}\eta_d \rho_l V_4^2 \tag{27}$$

6. Radiator

In the jet condenser, the coolant is used to remove the heat of condensation from the gaseous portion of the flow leaving the two-phase nozzle. For these calculations it is assumed that the coolant rejects heat in a radiator directly. If thermal effects are neglected in the coolant diffuser and nozzle (see Appendix), the waste heat radiated to space is given by

$$Q_{\text{rad}} = \dot{m}_c C_l (T_2 - T_8) = \dot{m}_g L \tag{28}$$

7. Cycle Efficiency

The cycle efficiency is the output power divided by the sum of the output power and the radiated power, or

$$\eta = \frac{P_e}{P_e + Q_{\text{rad}}} \tag{29}$$

8. Prime Radiator Area

The Stefan-Boltzmann law is used to calculate the area/kw of output power required to radiate the waste heat to space. In this cycle, the heat must be rejected by lowering the temperature of the coolant. If the heat rejected over each small increment of temperature change is integrated from the inlet to exit temperature, the following expression results for the effective radiating temperature:

$$T_{\text{eff}}^4 = \frac{3T_2^3 T_7}{1 + T_2/T_7 + (T_2/T_7)^2} \tag{30}$$

The prime radiator area is then expressed as

$$A_{\text{rad}} = \frac{Q_{\text{rad}}}{\sigma\,\varepsilon\,T_{\text{eff}}^4\,P_e} \tag{31}$$

9. Specific Weight

The equation for the specific weight,

$$W_s = C_1 + \frac{C_2}{\sqrt{\eta}} + C_3 A_{\text{rad}}$$

is the same equation (Eq. 12) presented in the analyses of the other cycles. The values of C_1, C_2, and C_3 are assumed to be the same as those presented in the other cycle analyses.

D. Two-Component Jet Condenser Cycle

Figure 5 presents two possible variations of the two-component jet condenser cycle. In the cycle represented

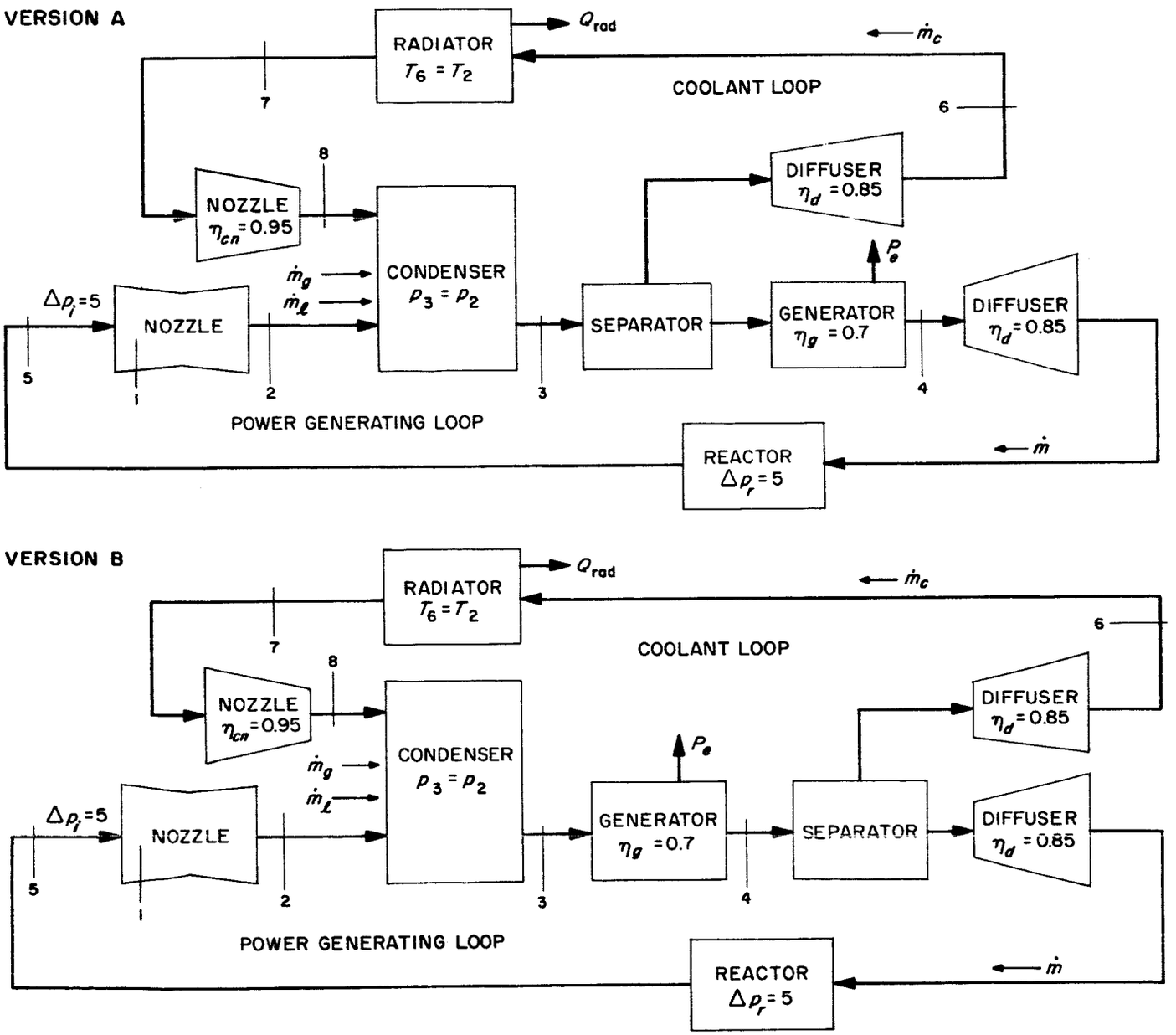

Fig. 5. Two-component jet condenser cycles

by Fig. 5a, a low quality flow of liquid metal such as Cs is expanded through a nozzle. The vapor from the nozzle exhaust is condensed in the jet condenser by the injection of a coolant consisting of a different species having high specific heat (e.g., Li). The resulting mixture, which is now all liquid, leaves the jet condenser with a velocity that is higher than the subcooled liquid injection velocity. The two liquids are separated, and the coolant passes through a diffuser to the radiator where the coolant is subcooled, accelerated in a nozzle to a high velocity, and then reinjected into the condenser. The liquid metal in the power generating loop (e.g., cesium) leaves the condenser and decelerates through the production of electric power in the MHD generator. The liquid then leaves the generator with sufficient velocity to return through a diffuser to the reactor where it is partially vaporized.

Figure 5b differs from Fig. 5a only in that the two liquids are separated after passing through the MHD generator, rather than before entering the generator.

The energy conversion steps and assumptions made in this analysis are the same as those made in the single-component jet condenser cycle analysis. Any energy loss

that would be incurred in separating the two liquid metals was not included.

Only two equations presented in the single-component jet condenser cycle analysis need be modified so that the physical properties of the coolant can be included. The two equations that are affected are Eq. (19)

$$\dot{m}_g L = \dot{m}_c C_l (T_2 - T_7)$$

and Eq. (17)

$$p_7 - p_2 = \tfrac{1}{2}\eta_d \rho_l V_3^2$$

where, now, $C_l = C_l$ (coolant) and $\rho_l = \rho_l$ (coolant).

Assumptions and analytical methods used in the cycle analyses are summarized in Table 1.

Table 1. Summary of cycle analysis assumptions and analytical methods

Parameter	Cycle		
	Two-component separator cycle	Single-component separator cycle	Jet condenser cycle
Pump efficiency	0.50	0.50	Not applicable
Diffuser efficiency	0.85	0.85	0.85
Coolant diffuser efficiency	Not applicable	Not applicable	0.85
Generator efficiency	0.70	0.70	0.70
Liquid nozzle efficiency	Not applicable	Not applicable	0.95
Nozzle injection pressure loss, psi	5	5	5
Reactor pressure loss, psi	5	5	5
Regenerative heat exchanger pressure loss, psi	5	Not applicable	Not applicable
Emissivity of the radiator surface	0.90	0.90	0.90
Separator or condenser friction loss	Analysis of Ref. 10	Analysis of Ref. 10	Analysis of Ref. 10
Two-phase nozzle performance	Analysis of Ref. 9	Analysis of Ref. 9	Analysis of Ref. 9
Jet condenser mixing performance	Not applicable	Not applicable	Constant pressure, liquid saturation at exit

III. METHOD OF COMPUTATION

The nozzle inlet pressure was taken as the saturation pressure at the maximum cycle temperature under consideration (for Cs-Li this was taken from Ref. 19). Nozzle exhaust conditions were calculated, from the appropriate nozzle program, for various nozzle inlet mass flow ratios of vapor to liquid. These conditions were used as inputs to programs incorporating the pertinent separator or condenser equations, with or without friction. For the cases with friction, the optimum separator or condenser angle was employed. Latent heats were evaluated at the condensing temperature, and densities and specific heats were evaluated at the mean temperatures for each process. The cycle efficiencies, prime radiator areas, and specific weights calculated for each component mass ratio, R, were plotted as a function of nozzle exhaust pressure to find the minimum prime radiator area, the minimum specific weight, and the maximum cycle efficiency. An example of this procedure is given in Fig. 6,

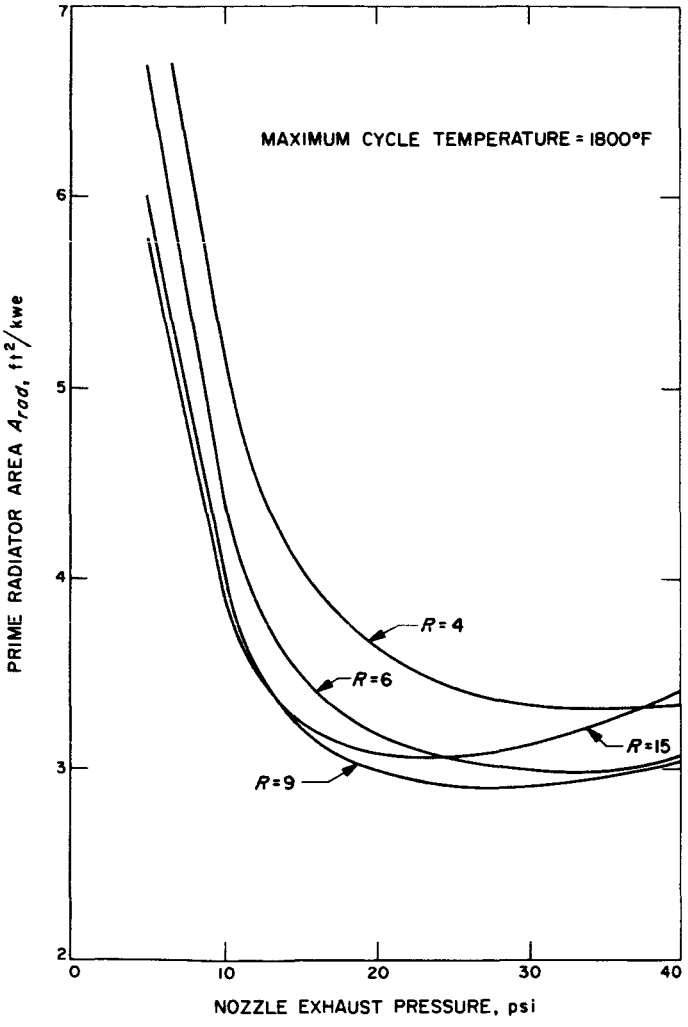

Fig. 6. Effect of nozzle exhaust pressure on prime radiator area with mass flow ratio as parameter

in which a mass ratio of 9 can be seen to give the minimum, or near minimum, prime radiator area for all exhaust pressures, and is, thereby, the optimum mass ratio for minimizing area. The cycle efficiency calculated at each nozzle exhaust pressure for this mass ratio was then plotted against the corresponding prime radiator area, resulting in curves such as those presented in Fig. 7.

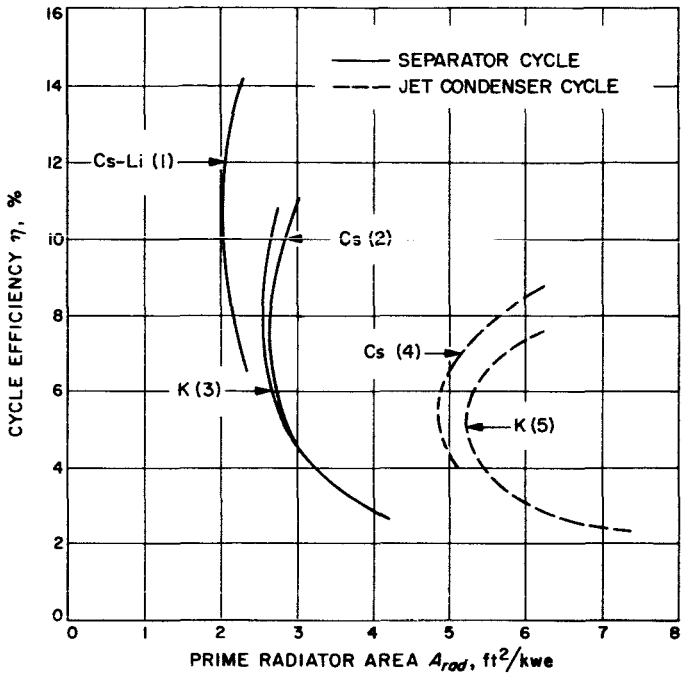

Fig. 7. Variation of cycle efficiency with prime radiator area at 1800°F, without friction

This procedure was also followed in deriving curves of efficiency vs specific weight (such as shown in Fig. 13).

Two sets of thermophysical property data exist for potassium, one published by Battelle Memorial Institute (Ref. 20) and the other by the Naval Research Laboratory (Ref. 21). It was found that no more than a 0.1-percentage-point difference occurred in the cycle efficiency for any given prime radiator area or specific weight.

Properties reported by Battelle were the ones arbitrarily chosen for use in the investigation of single- and two-component cycles using potassium. The property data of Ref. 22 was used in the investigation of single- and two-component cycles using cesium. Properties of lithium were obtained from Refs. 23 and 24. Solubilities were obtained from Ref. 25.

IV. CYCLE COMPARISON

The criteria chosen to compare the four types of liquid MHD cycles are cycle efficiency, system weight, and prime radiator area, where prime radiator area is defined as area/kwe necessary to reject the cycle waste heat, assuming no temperature difference between fluid and radiator surface. All of these parameters must be considered, since they are all important for determining the performance of a space power system. Comparisons made on the basis of any parameter, alone, would not provide sufficient information to choose from among the available systems. A system having the highest cycle efficiency, for example, could still have a significantly larger radiator area and a higher weight than a system with somewhat lower efficiency. Thus, a choice would have to be made by the power system user as to the relative importance of these parameters. Higher cycle efficiency would of course mean that a smaller reactor would be required for a given power output. This would be important if the reactor were a developed item that had a fixed power rating. A lower power generating system weight would increase the payload capabilities for a given booster and mission, while a small radiator area would facilitate the packaging of the system.

To compare cycle performances, the maximum cycle efficiency, minimum system weight and minimum prime radiator area were individually determined at maximum cycle temperatures of 1800, 2000, and 2200°F for all cycles—with the exception of the two-component jet condenser cycles. The performance of the latter was determined only at 2000°F. A number of different working fluids were considered. Cesium-lithium and potassium-lithium were investigated as working fluid combinations for the two-component separator cycle. Potassium and cesium were each considered for the single-component separator and jet condenser cycles, while cesium-lithium was the fluid combination investigated for both versions of the two-component jet condenser cycle.

In the subsequent discussion, the cycles will be designated as follows:

Cycle 1	Cesium-lithium separator cycle
Cycle 2	Cesium separator cycle
Cycle 3	Potassium separator cycle
Cycle 4	Cesium jet condenser cycle
Cycle 5	Potassium jet condenser cycle
Cycle 6	Cesium-lithium jet condenser cycle (version A)
Cycle 7	Cesium-lithium jet condenser cycle (version B)
Cycle 8	Potassium-lithium separator cycle

A. Relationship Between Cycle Efficiency and Radiator Area Without Friction

Figures 7, 8, and 9 illustrate the performance differences of the cycles without separator or condenser friction at 1800, 2000, and 2200°F. Each point on the curves is at a different exit pressure, decreasing from about 30% of nozzle inlet pressure at the lower end of the curves to about 2% at the other end. Initially, the cycles follow Rankine cycle behavior of increasing cycle efficiency and decreasing radiator area, until a radiator temperature equal to about 75% of the nozzle inlet temperature is reached, beyond which the radiator area again increases.

Figure 7 shows the relation between cycle efficiency and radiator area at 1800°F for the separator and single-component jet condenser cycles. Cycle 1 has the smallest prime radiator area which is 2.1 ft²/kwe at 9 to 12%

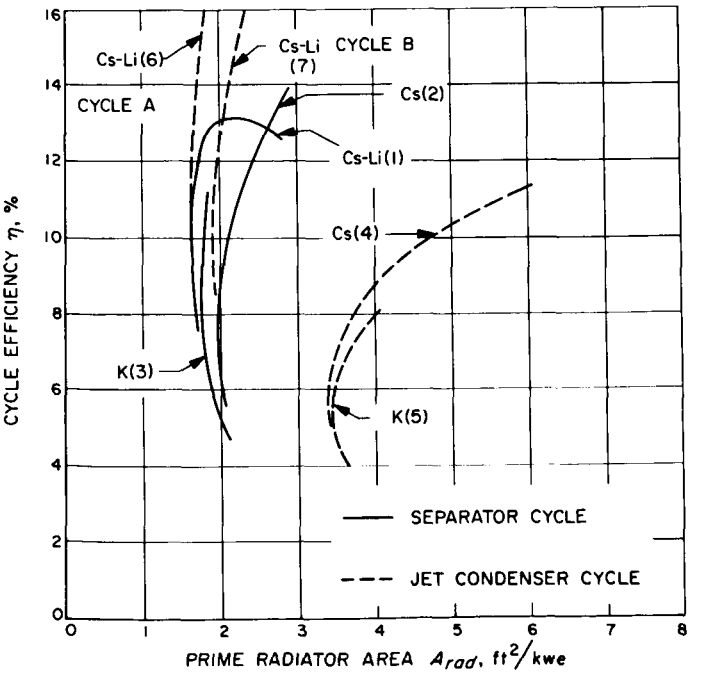

Fig. 8. Variation of cycle efficiency with prime radiator area at 2000°F, without friction

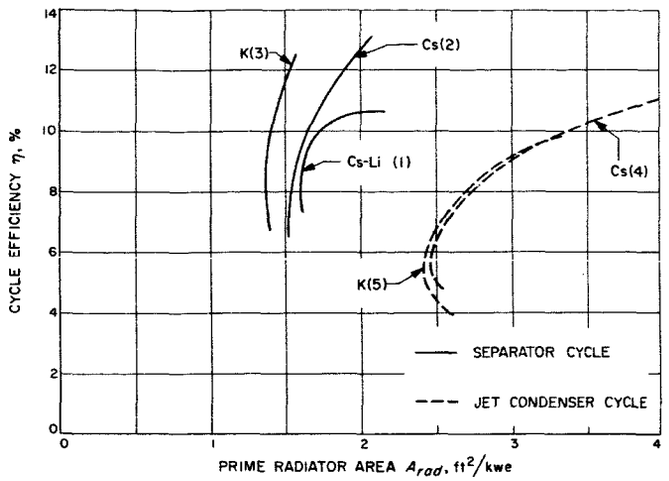

Fig. 9. Variation of cycle efficiency with prime radiator area at 2200°F, without friction

cycle efficiency. Cycles 2 and 3 have larger radiator areas. The better performance exhibited by cycle 1 is the result of the high heat capacity of lithium which provides near-isothermal nozzle flow (Li temperature drop is only about 50°F) and, consequently, near-isothermal heat addition in the reactor, which thermodynamically, is the most efficient situation. In cycles 2 and 3, on the other hand, the reactor must heat the liquid all the way from the radiator exit temperature to the maximum cycle temperature, a 600 to 1000°F temperature rise, with lower availability of the heat input than for an isothermal process. Disadvantages of the near-isothermal liquid flow in the two-component cycle are the superheat of the exhaust vapor, which requires using a regenerative heat exchanger for maximum efficiency, and the high temperature of the liquid metal flowing through the generator.

The single-component jet condenser cycles (cycles 4 and 5) suffer from the same non-ideal heat input as the single-component separator cycles (cycles 2 and 3). Also, an energy loss results from mixing streams of different velocities and from the variable-temperature heat rejection which takes place at an average temperature that is lower than the nozzle exhaust saturation temperature. As a consequence of lower heat rejection temperature and low energy efficiencies for the jet condenser, a larger radiator area is required than for cycles 2 and 3.

Figure 8 compares all of the cycles, including the Cs-Li jet condenser cycles, at 2000°F. A minimum radiator area of 1.6 ft²/kwe is achieved by both the Cs-Li separator cycle (cycle 1) and cesium-lithium jet condenser cycle (cycle 6) at efficiencies of 9 to 12%. Slightly larger areas of 1.8 ft²/kwe and 1.9 ft²/kwe result for the single-component separator cycles (cycles 2 and 3). These minima occur at efficiencies of about 8%. Cycle 7 has a minimum area of 1.9 ft²/kwe at efficiencies of 9 to 12%. The single-component condenser cycles (cycles 4 and 5) show minimum areas of 3.4 ft²/kwe at a cycle efficiency of 6%.

In all cycles, with the exception of cycle 1, a continuous increase in efficiency may be obtained by lowering the nozzle exhaust pressure (increasing radiator area). Cycle 1 reaches a maximum efficiency of 13%, then decreases as the nozzle exhaust pressure is further reduced. This decrease is due to an increase in the percentage of Li carried over to the radiator, which increases the heat rejection.

Cycles 6 and 7 achieve higher cycle efficiencies than do cycles 4 and 5 because the large heat capacity of Li reduces the amount of coolant required by a factor of 4, or more. Kinetic energy losses in the jet condenser are thereby reduced, resulting in an increase in the output power. Smaller radiator areas are needed, since the high heat capacity of lithium permits the waste heat to be radiated at a higher average temperature.

Figure 9 shows the cycle performances at 2200°F. Increased radiator temperatures result in reduction of the prime radiator area for cycles 2 and 3 but not for cycle 1. Cycle 1 performance is degraded at this temperature by increased equilibrium Cs solubility in Li, estimated as 16% at 2200°F vs 7.3% at 2000°F, and by increased Li vapor pressure. The high solubility causes an increase in Cs vapor flow rate as the mixture expands through the nozzle, reducing the average pressure ratio for the Cs; and the increased Li vapor pressure increases the Li flow to the radiator.

B. Relationship Between Cycle Efficiency and Radiator Area With Friction

Cycle performances, including the effect of friction, are plotted in Figs. 10, 11, and 12. Figure 10 compares cycle performances at 1800°F. Cycle 1 has a minimum area of 2.9 ft²/kwe and a maximum cycle efficiency of 7.5%. The 1800°F minimum area without friction was 2.1 ft²/kwe at 9 to 12% efficiency; thus, separator friction is an acceptable loss in this cycle. The loss in performance with the single-component separator cycles (cycles 2 and 3) when friction is considered is much greater than for cycle 1, because of less efficient separator performance (as discussed later). The best single-component separator cycle, cycle 2, has a minimum area of 4.8 ft²/kwe and peak efficiency of only 3.5%.

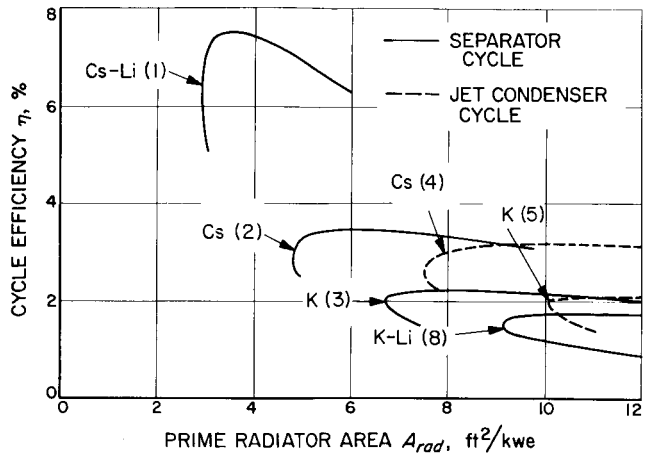

Fig. 10. Variation of cycle efficiency with prime radiator area at 1800°F, with friction

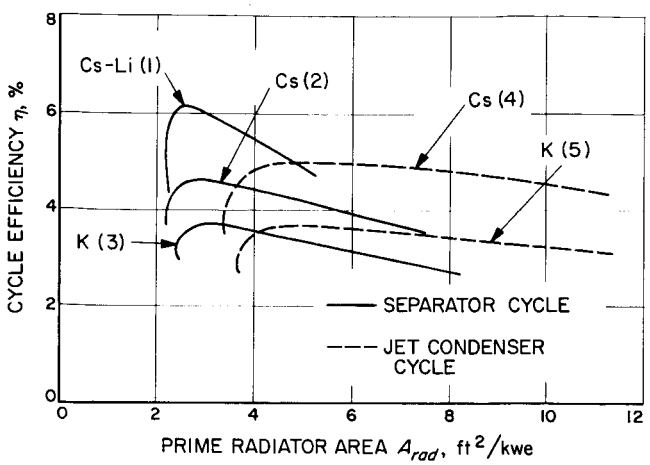

Fig. 12. Variation of cycle efficiency with prime radiator area at 2200°F, with friction

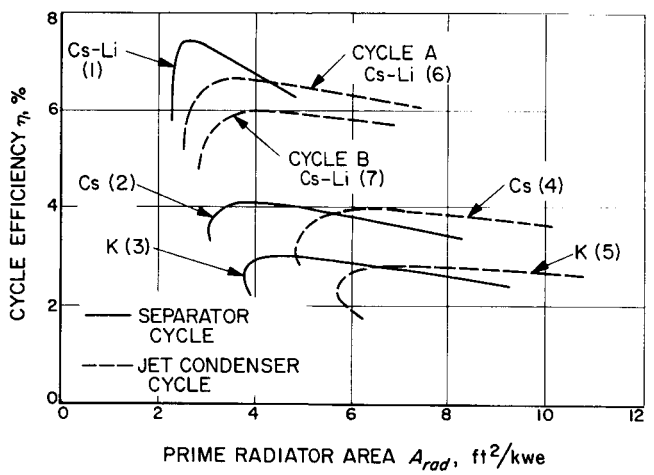

Fig. 11. Variation of cycle efficiency with prime radiator area at 2000°F, with friction

All cycles have an upper limit to cycle efficiency when friction is considered. This is due to the increase in separator area required as the nozzle exhaust pressure is reduced. The performance of the other two-component separator cycle (cycle 8) is low, because of the very high solubility of potassium in Li (Ref. 25). Since the solubility increases with temperature, this cycle was not considered at higher temperatures.

At 2000°F, Fig. 11 shows that the minimum radiator area of cycle 1 has been reduced to 2.3 ft²/kwe, while the maximum cycle efficiency remains 7.5%. The performances of cycles 2, 3, 4, and 5 have improved. Cycle 6 has a minimum prime radiator area of 2.5 ft²/kwe and a maximum cycle efficiency of 6.7%.

At 2200°F, Fig. 12 shows that cycle 1 still exhibits the best performance, although the maximum cycle efficiency has dropped to 6.1%.

C. Relationship Between Cycle Efficiency and Specific Weight

Plots were made to show the variation of cycle efficiency with specific weight at 2000°F, both with and without separator or condenser friction. The same optimization procedure with respect to nozzle exhaust pressure that was discussed previously for radiator area was also used for specific weight. Figure 13 shows the results without friction; on comparison with Fig. 8, it can be seen that the order of increasing weights among the cycles is the same as the order of increasing areas, and that minimum weight occurs at radiator areas about 10% above the minimum area. The same is true with friction included, as shown in Fig. 14. The minimum weight for cycle 1 with separator friction is 26 lb/kwe vs 21 lb/kwe without separator friction.

D. Variation of Radiator Area with Maximum Cycle Temperature

The influence of reactor temperature on the minimum prime radiator area is shown in Fig. 15, in which cycle 1 data have been extended to 1600°F. Temperature has a marked influence because of the fourth power dependence of radiator area. For the two-component separator cycle, the minimum prime area attainable falls from

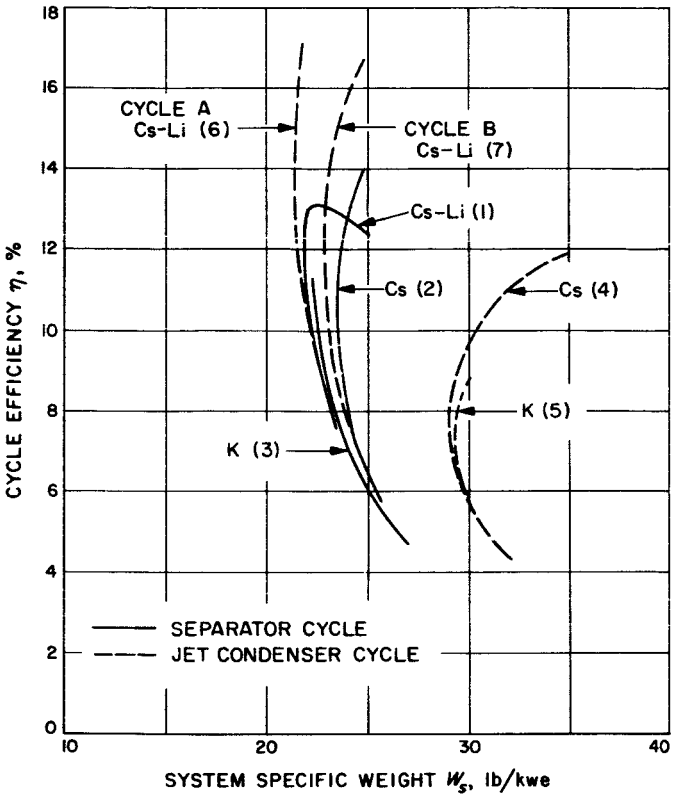

Fig. 13. Variation of cycle efficiency with system specific weight at 2000°F, without friction

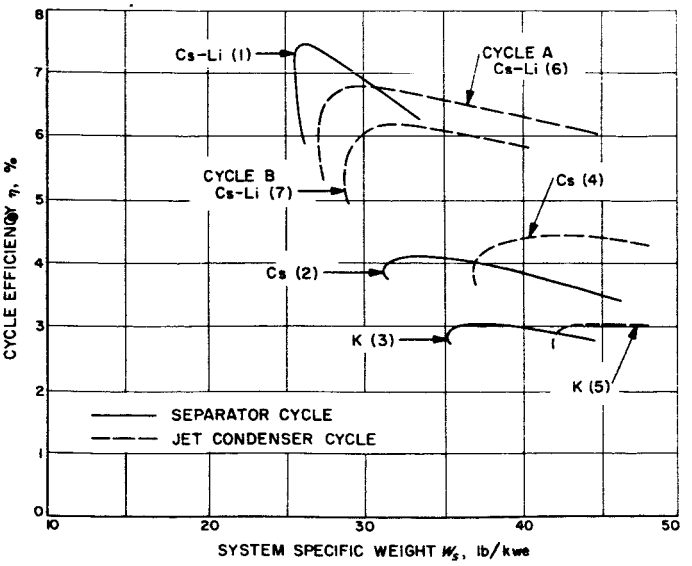

Fig. 14. Variation of cycle efficiency with system specific weight at 2000°F, with friction

4.7 ft²/kwe at 1600°F to 2.2 ft²/kwe at 2200°F. The single-component (Cs) separator cycle changes from 4.8 ft²/kwe at 1800°F to 2.2 ft²/kwe at 2200°F. The

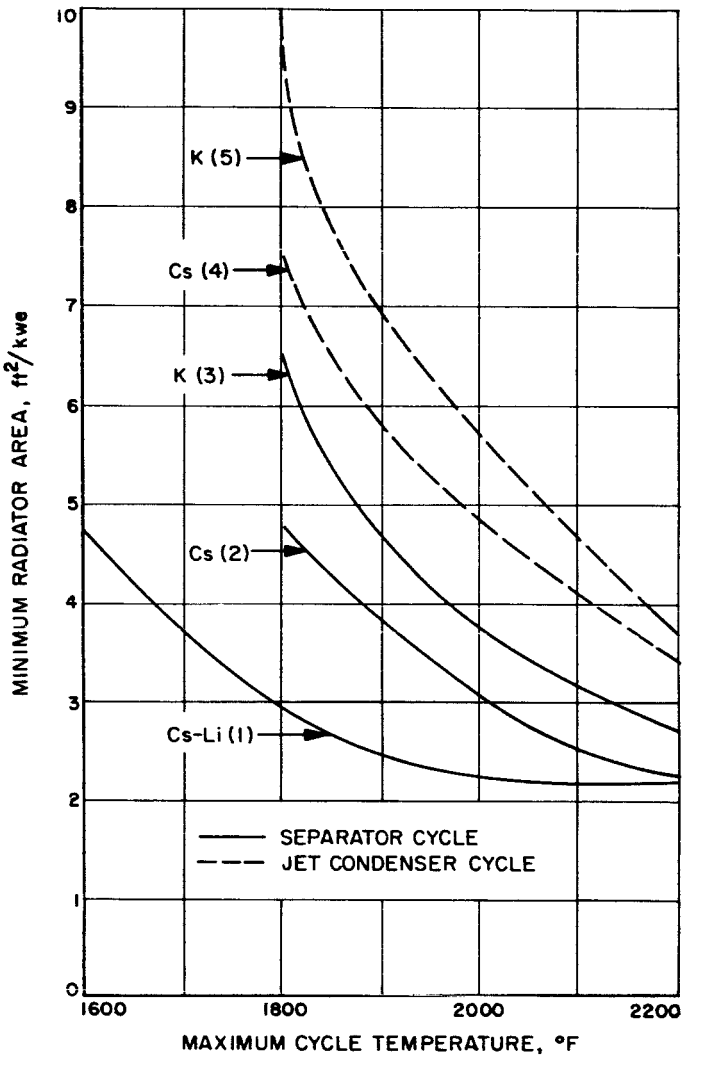

Fig. 15. Effect of maximum cycle temperature on minimum radiator area

reduction in prime radiator area is less pronounced for the two-component system than for the single-component system, because of the increase in solubility of cesium in lithium with temperature. This increased solubility lowers the efficiency and results in an increase in the total heat rejected.

E. Variation of Cycle Efficiency with Maximum Cycle Temperature

The maximum efficiencies of cycles 1 through 5 are plotted as a function of maximum cycle temperature in Fig. 16. The efficiency of the two-component separator cycle using the Cs-Li combination decreases with temperature above 2000°F because of the solubility effect discussed previously.

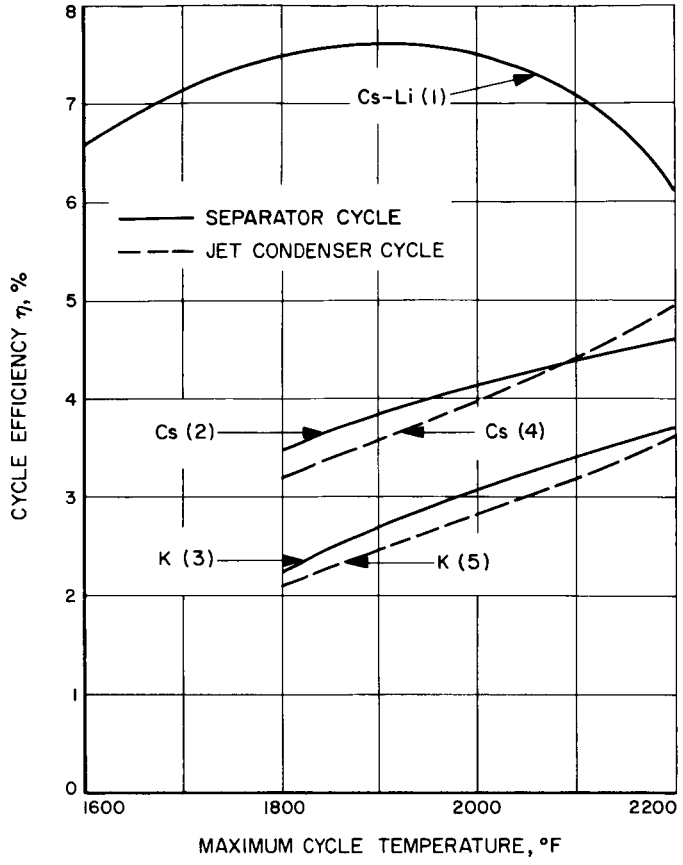

Fig. 16. Effect of maximum cycle temperature on cycle efficiency, with friction

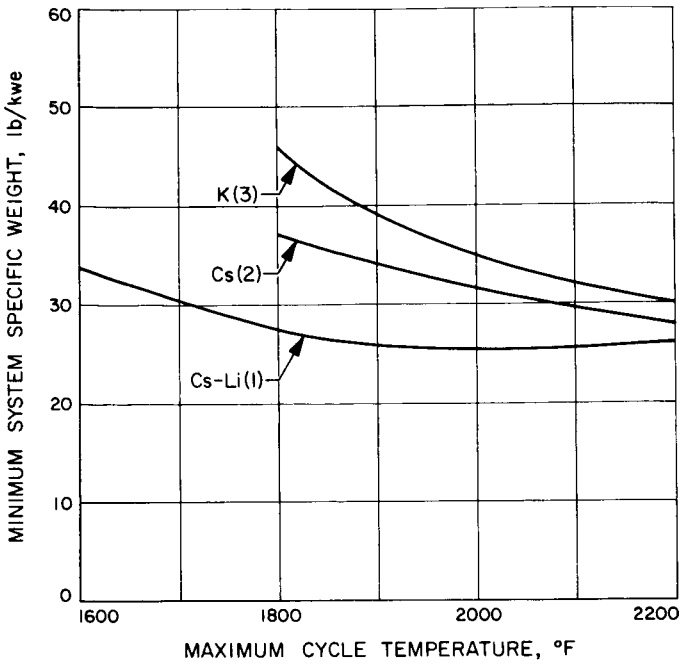

Fig. 17. Effect of maximum cycle temperature on minimum specific weight of separator cycles, with friction

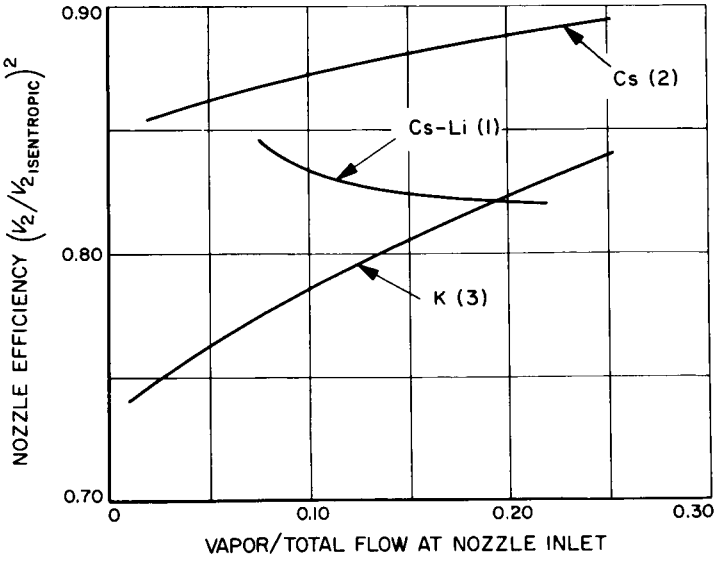

Fig. 18. Variation of nozzle efficiency with the ratio of vapor to total flow at the nozzle inlet for separator cycles at 2000°F

F. Variation of Minimum Specific Weight with Maximum Cycle Temperature

The variation of minimum specific weight with the maximum cycle temperature for the three separator cycles (cycles 1, 2, and 3) is shown in Fig. 17. The minimum specific weight decreases continuously with increasing cycle temperature for cycles 2 and 3 because of the improved cycle efficiency and smaller radiator area required. Since the efficiency of cycle 1 decreases at 2200°F, there is a small increase in the specific weight over that at 2000°F. Cycle 1, however, still has the lowest specific weight at all temperatures considered.

G. Component Performance

Examination of the nozzle and separator efficiencies reveals one of the reasons for the large gap in efficiency between cycle 1 and the other cycles when the friction is included. Figure 18 shows the nozzle efficiency (fraction of isentropic kinetic energy attained) over the range of optimum inlet flow ratios at 2000°F at a typical nozzle exit pressure of 15 psi. The highest nozzle efficiency is obtained with Cs, although not by a large margin; the efficiency is 0.87 as compared with 0.83 for the Cs-Li mixture and 0.79 for K at a mixture ratio of 0.1.

This advantage of Cs is not pronounced enough to compensate for the Cs separator performance. Figure 19 shows the separator efficiency for the three cases. At a flow ratio of 0.10, the Cs-Li separator has an efficiency of 0.85 vs 0.72 for the Cs, while it is only 0.63 for K. These values result from the differing nozzle exit areas, velocities, and liquid densities.

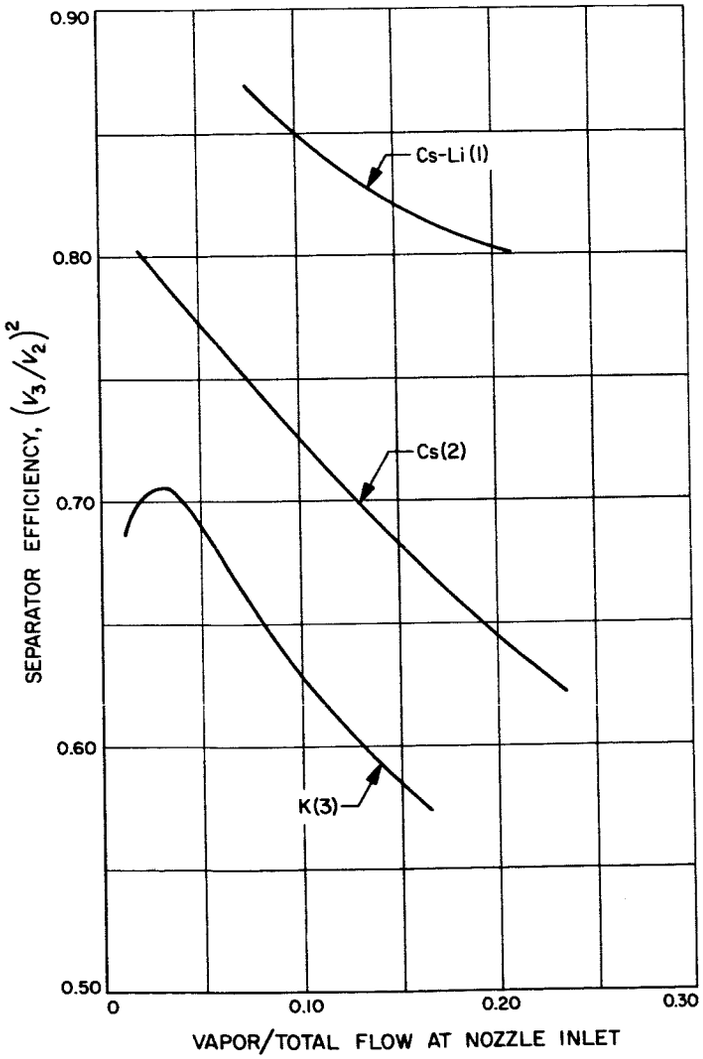

Fig. 19. Variation of separator efficiency with the ratio of vapor to total flow at the nozzle inlet for separator cycles at 2000°F

The product of nozzle and separator efficiency is given in Fig. 20. These curves show one reason for the cycle efficiency advantage of the Cs-Li system in that the combined nozzle-separator efficiency is about 8 percentage points higher than for the Cs system and about 20 percentage points higher than for the K system.

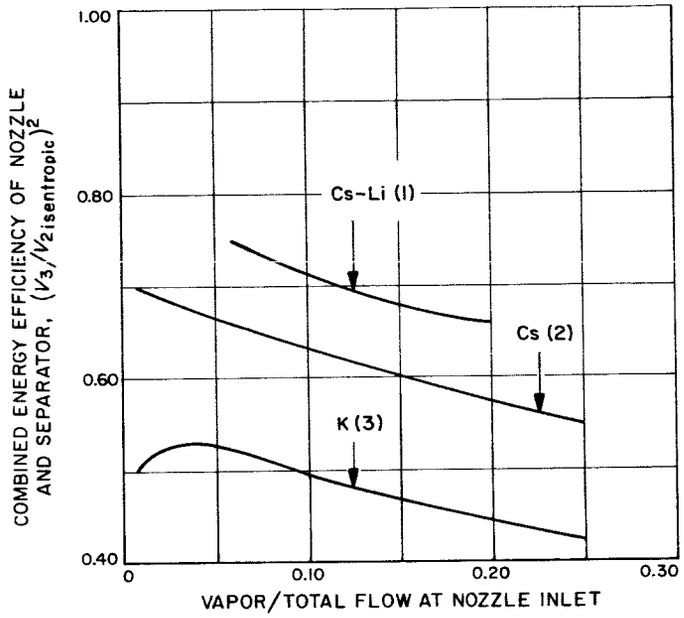

Fig. 20. Variation of the combined nozzle-separator efficiency with the ratio of vapor to total flow at the nozzle inlet for separator cycles at 2000°F

Figure 21 shows how the performance of jet condenser cycles is affected by varying the fraction of liquid that impinges on the walls of the jet condenser. The cycle chosen for this study is the best condenser cycle, cycle 6, at 2000°F (with component ratio held constant rather than optimized as in the previous figures). It can be seen that, even if only 20% of the liquid impinges on the

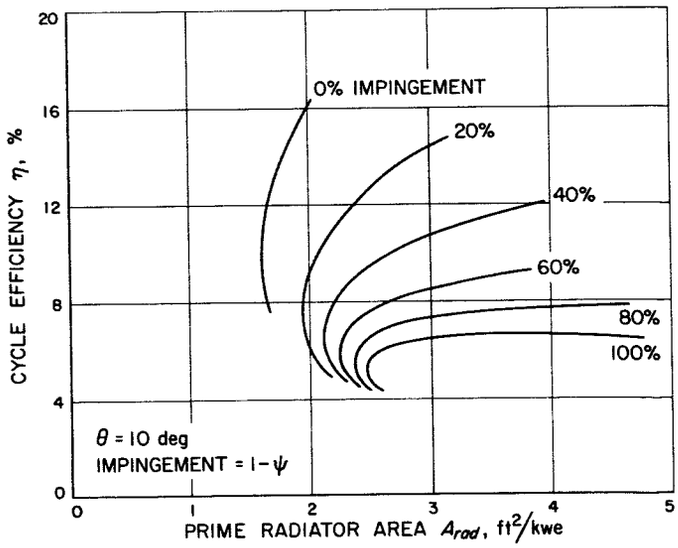

Fig. 21. Effect of liquid impingement fraction on cycle efficiency and radiator area of Cs-Li condenser cycle (cycle B) at 2000°F

walls, the cycle efficiency at the minimum radiator area drops from an efficiency of 10% to 8%. The minimum area increases from 1.6 ft²/kwe with no impingement to 1.9 ft²/kwe at 20% impingement. Figure 22 has plots of the cycle efficiency at the minimum area and an arbitrary area of 2.5 ft²/kwe vs the fraction of liquid that impinges on the jet condenser walls. Both curves show that half the loss in cycle efficiency occurs within the first 25% of wall impingement.

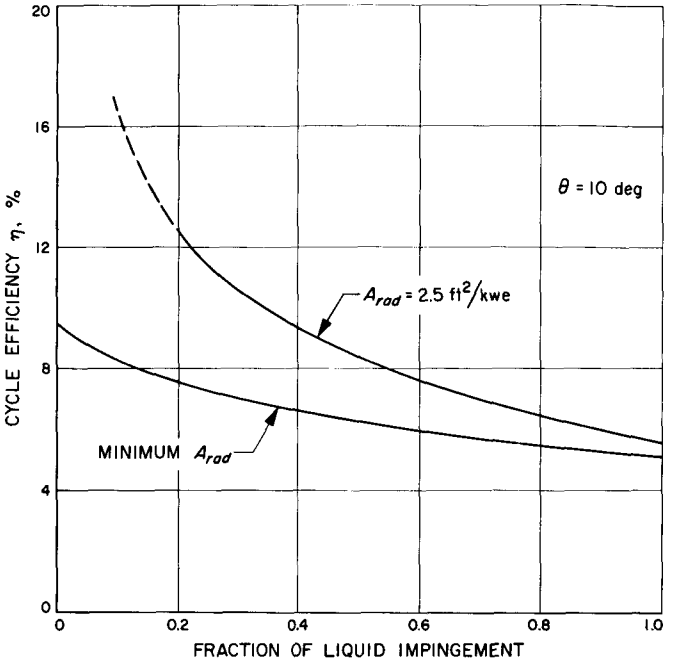

Fig. 22. Variation of cycle efficiency with liquid impingement fraction (cycle B)

The results of an experiment to investigate the possibility of eliminating impingement friction are discussed in Ref. 18. In this experiment, the nozzle geometry was such that the flow was intended to coalesce in a free jet without wall impingement. Some increase in liquid concentration was observed, indicating a possible avenue toward low-friction condensers and separators. However, typical experimental results for jet condensers—even operating with high quality vapor flow—show only 70 to 85% of the predicted performance (Refs. 15 and 16). The performance of the jet condenser would be further reduced from that calculated here, since the simplifying assumption was made that the exit liquid temperature is equal to the vapor temperature. This condition is possible only if an infinite length is used to effect complete vapor condensation (Ref. 17). Instead, the liquid exit temperature must be about 50°F lower than the vapor temperature, making the radiator area approximately 10% greater than the values calculated.

A summary of the cycle parameters, without friction and with friction, are presented in Tables 2 and 3, respectively.

Table 2. Summary of cycle performance without separator and condenser friction

Maximum cycle temp., °F	Cycle No.	Min. A_{rad}, ft²/kwe	Max. η, %	Min. W_s, lbm/kwe
1800°F	1	2.1	No maximum	Not calculated
	2	2.6	No maximum	Not calculated
	3	2.5	No maximum	Not calculated
	4	4.9	No maximum	Not calculated
	5	5.2	No maximum	Not calculated
2000°F	1	1.6	13.1	21.8
	2	2.0	No maximum	23.6
	3	1.7	No maximum	22.3
	4	3.4	No maximum	29.1
	5	3.4	No maximum	29.4
	6	1.6	No maximum	21.5
	7	1.9	No maximum	22.9
2200°F	1	1.6	10.6	Not calculated
	2	1.5	No maximum	Not calculated
	3	1.4	No maximum	Not calculated
	4	2.5	No maximum	Not calculated
	5	2.4	No maximum	Not calculated

Table 3. Summary of cycle performance with separator and condenser friction

Maximum cycle temp., °F	Cycle No.	Min. A_{rad}, ft²/kwe	Max. η, %	Min. W_s, lbm/kwe
1800°F	1	2.9	7.5	Not calculated
	2	4.8	3.5	Not calculated
	3	6.7	2.2	Not calculated
	4	7.5	3.2	Not calculated
	5	10.1	2.1	Not calculated
	8	9.2	1.8	Not calculated
2000°F	1	2.2	7.5	25.7
	2	3.0	4.1	31.2
	3	3.8	3.0	35.2
	4	4.8	4.0	37.0
	5	5.7	2.8	41.8
	6	2.5	6.7	27.2
	7	2.8	6.0	28.7
2200°F	1	2.2	6.1	Not calculated
	2	2.2	4.6	Not calculated
	3	2.4	3.7	Not calculated
	4	3.4	4.9	Not calculated
	5	3.6	3.7	Not calculated

V. CONCLUSIONS

From the comparison of liquid-metal MHD power conversion cycles investigated in this study, two principal conclusions may be drawn for operation when separator and condenser friction and deflection are included (100% impingement). First, two-component cycles—both separator and condenser—have maximum efficiencies of 6 to 7%, as compared with single-component cycles with maximum efficiencies of only 3 to 4%. Second, the two-component separator cycle has a slightly higher efficiency and smaller radiator area than the two-component condenser cycles.

For operation without separator and condenser friction or deflection, there were three findings. First, all of the cycles studied are capable of efficiencies greater than 10%. Second, for a given efficiency, the two-component cycles require about half as much radiator area as do the single-component cycles. And third, the efficiency of the two-component condenser cycles increases indefinitely with decreasing rejection temperature, while the efficiency of the two-component separator cycle is limited to 13%.

It thus appears that the most promising cycle for space applications is the two-component (cesium-lithium) separator cycle, if substantially 100% liquid impingement must be accepted in both jet condensers and separators. The two-component (cesium-lithium) condenser cycles appear promising for ultimate high efficiency, should it be possible to substantially eliminate impingement in condensers.

APPENDIX

Heat Radiated in the Jet Condenser Cycle

In this Appendix, it will be shown that the use of $\dot{m}_g L$ for the heat rejection in the condenser cycle is a satisfactory approximation.

1. Coolant Diffuser

The energy balance between the entrance and exit of the coolant diffuser, per pound of coolant, is as follows:

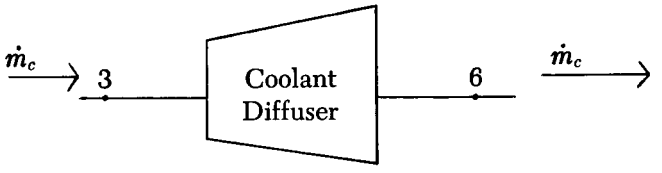

$$h_6 + \frac{V_6^2}{2g_cJ} = h_3 + \frac{V_3^2}{2g_cJ} \tag{A-1}$$

where J is the mechanical equivalent of heat.

Substitution of the definition of enthalpy of a liquid in Eq. (A-1) gives:

$$C_l T_6 + \frac{p_6}{\rho_l} + \frac{V_6^2}{2g_cJ} = C_l T_3 + \frac{p_3}{\rho_l} + \frac{V_3^2}{2g_cJ} \tag{A-2}$$

From combination of terms,

$$C_l(T_6 - T_3) = \frac{(V_3^2 - V_6^2)}{2g_cJ} - \frac{p_6 - p_3}{\rho_l} \tag{A-3}$$

and substitution of the definition of η_d,

$$\eta_d = \frac{2(p_6 - p_3)}{\rho_l(V_3^2 - V_6^2)}$$

Eq. (A-3) becomes

$$C_l(T_6 - T_3) = \frac{(V_3^2 - V_6^2)}{2g_cJ} - \frac{\eta_d(V_3^2 - V_6^2)}{2g_cJ} = \frac{(1 - \eta_d)}{2g_cJ}(V_3 - V_6^2) \tag{A-4}$$

Since $T_3 = T_2$, and $V_6 \approx 0$,

$$C_l(T_6 - T_2) = \frac{(1 - \eta_d)V_3^2}{2g_cJ} = \frac{(1 - \eta_d)V_2^2}{2g_cJ[1 + (0.1\,\dot{m}_c/\dot{m})]^2} \tag{A-5}$$

2. Coolant Nozzle

The energy balance between the entrance and exit of the coolant nozzle is given by:

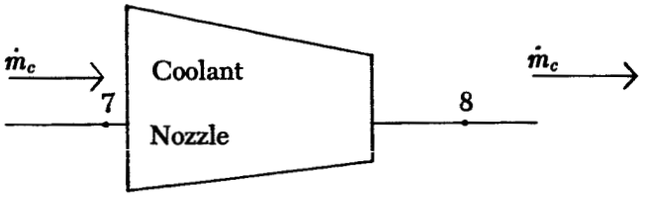

$$h_8 + \frac{V_8^2}{2g_cJ} = h_7 + \frac{V_7^2}{2g_cJ} \tag{A-6}$$

Substitution of the definition of enthalpy of a liquid into Eq. (A-6) gives

$$C_l T_8 + \frac{p_8}{\rho_l} + \frac{V_8^2}{2g_cJ} = C_l T_7 + \frac{p_7}{\rho_l} + \frac{V_7^2}{2g_cJ} \tag{A-7}$$

By combining terms,

$$C_l(T_8 - T_7) = \frac{V_7^2 - V_8^2}{2g_cJ} - \frac{p_8 - p_7}{\rho_l} \tag{A-8}$$

and substituting the definition of η_{cn},

$$\eta_{cn} = \frac{\rho_l(V_8^2 - V_7^2)}{2(p_7 - p_8)} ,$$

$$C_l(T_8 - T_7) = -\frac{V_8^2 - V_7^2}{2g_cJ} + \frac{V_8^2 - V_7^2}{2g_cJ\,\eta_{cn}} = \frac{V_8^2 - V_7^2}{2g_cJ}\left(\frac{1}{\eta_{cn}} - 1\right) \tag{A-9}$$

Since $V_7 \approx 0$ and

$$V_8^2 = \frac{2\eta_{cn}}{\rho_l}(p_7 - p_8) = \frac{2\eta_{cn}}{\rho_l}(p_6 - p_3) = \eta_{cn}\,\eta_d\,V_3^2 = 0.81V_3^2 \tag{A-10}$$

Therefore,

$$C_l\,(T_8 - T_7) = \frac{1 - \eta_{cn}}{2\eta_{cn}g_cJ}\,\eta_{cn}\,\eta_d\,V_3^2 \tag{A-11}$$

and finally,

$$C_l(T_8 - T_7) = \frac{(1 - \eta_{cn})\,\eta_d\,V_2^2}{2g_cJ[1 + (0.1\,\dot{m}_c/\dot{m})]^2} \tag{A-12}$$

3. Jet Condenser

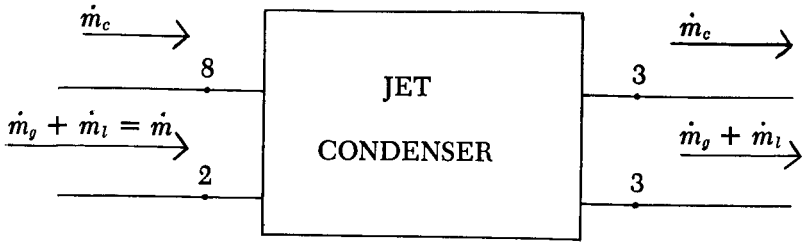

If constant pressure mixing is assumed, the energy balance across the jet condenser is

$$\dot{m}_c h_8 + \frac{\dot{m}_c V_8^2}{2g_c J} + \dot{m}_g L_2 + \dot{m} h_2 + \frac{\dot{m} V_2^2}{2g_c J} = (\dot{m}_c + \dot{m}) \left(h_3 + \frac{V_3^2}{2g_c J} \right) \tag{A-13}$$

By substituting for enthalpy,

$$\dot{m}_c C_l T_8 + \frac{\dot{m}_c V_8^2}{2g_c J} + \dot{m}_g L_2 + \dot{m} C_l T_2 + \frac{\dot{m} V_2^2}{2g_c J} = (\dot{m}_c + \dot{m}) \left(C_l T_3 + \frac{V_3^2}{2g_c J} \right) \tag{A-14}$$

where pressure terms have cancelled out because of the assumption of constant-pressure. Since $T_2 = T_3$, the saturation temperature at the condenser pressure,

$$\dot{m}_c C_l T_8 + \frac{\dot{m}_c V_8^2}{2g_c J} + \dot{m}_g L_2 + \frac{\dot{m} V_2^2}{2g_c J} = \dot{m}_c C_l T_2 + \frac{\dot{m}_c V_3^2}{2g_c J} + \frac{\dot{m} V_3^2}{2g_c J}$$

Combination of terms gives

$$\dot{m}_c C_l (T_2 - T_8) = \frac{\dot{m}_c (V_8^2 - V_3^2)}{2g_c J} + \frac{\dot{m} (V_2^2 - V_3^2)}{2g_c J} + \dot{m}_g L_2 \tag{A-15}$$

Use of Eq. (A-10) and $V_3 = V_2/[1 + (0.1\, \dot{m}_c/\dot{m})]$,

$$\dot{m}_c C_l (T_2 - T_8) = \frac{\dot{m}_c}{2g_c J} (0.81\, V_3^2 - V_3^2) + \frac{\dot{m}}{2g_c J} (V_2^2 - V_3^2) + \dot{m}_g L_2$$

$$= -\frac{0.19\, \dot{m}_c}{2g_c J} \left[\frac{V_2}{1 + (0.1 \dot{m}_c/\dot{m})} \right]^2 + \frac{\dot{m}}{2g_c J} \left(V_2^2 - \frac{V_2^2}{[1 + (0.1\, \dot{m}_c/\dot{m})]^2} \right) + \dot{m}_g L_2 \tag{A-16}$$

Finally,

$$\dot{m}_c C_l (T_2 - T_8) = \frac{V_2^2}{2g_c J} \left(\dot{m} - \frac{\dot{m} + 0.19 \dot{m}_c}{[1 + (0.1\, \dot{m}_c/\dot{m})]^2} \right) + \dot{m}_g L_2 \tag{A-17}$$

4. Radiator

The amount of heat rejected by the radiator is

$$Q_{rad} = \dot{m}_c C_l (T_6 - T_7) = \dot{m}_c C_l \left[(T_6 - T_2) + (T_8 - T_7) + (T_2 - T_8)\right] \tag{A-18}$$

From substitution of Eqs. (A-5), (A-12), and (A-17) in Eq. (A-18),

$$\dot{m}_c C_l (T_6 - T_7) = \frac{\dot{m} V_2^2}{2 g_c J} \left\{ 1 - \frac{1 + (0.19 \dot{m}_c/\dot{m})}{[1 + (0.1 \dot{m}_c/\dot{m})]^2} + \frac{\dot{m}_c}{\dot{m}} \left[\frac{(1 - \eta_d)}{[1 + (0.1 \dot{m}_c/\dot{m})]^2} + \frac{(1 - \eta_{cn})\,\eta_d}{[1 + (0.1 \dot{m}_c/\dot{m})]^2} \right] \right\} + \dot{m}_g L_2 \tag{A-19}$$

To determine the magnitude of the terms neglected in the cycle analysis, a data point was arbitrarily chosen for each of the single-component jet condenser cycles investigated. For Cs, the conditions giving the minimum area at 2000°F were substituted into Eq. (A-19). The conditions leading to the minimum specific weight at 2000°F were used for K.

5. Examples

The minimum area point for the cesium jet condenser cycle occurs at a nozzle inlet quality of 0.20 and $p_2 = 55.8$ psia. For this point, the following values were obtained:

$V_2 = 676.2$ ft/sec

$\dot{m}_c = 270.5$ lb/sec

$\dot{m} = 100$ lb/sec

$\eta_d = 0.85$

$\eta_n = 0.95$

$\dot{m}_g = 28.3$ lb/sec

$C_l = 0.059$ Btu/lb–°R

$L_2 = 206.7$ Btu/lb

$T_2 = 1996$°R

$T_7 = 1636$°R

Substitution of these values into Eq. (A-19) gives $Q_{rad} = 6203$ Btu/sec, which is only 6% greater than $\dot{m}_g L_2$.

The temperature T_6 is higher than T_2 by:

$$T_6 - T_2 = \frac{V_2^2 (1 - \eta_d)}{2 g_c J\, C_l \left[1 + (0.1 \dot{m}_c/\dot{m})\right]^2} = 14.4°\text{F}$$

This is about 14.4/1816 = 0.8% of the average radiator temperature. Thus, the area/unit radiated power is reduced by 3.2% (fourth-power dependence), but the heat rejected is increased by 6%, giving a required area increase of 2.8%.

For potassium, the minimum weight point occurs at a nozzle inlet quality of 0.20, and $p_2 = 28.3$ psia. For this point, the following values are found:

$V_2 = 1228$ ft/sec

$\dot{m}_c = 286.1$ lb/sec

$\dot{m} = 100$ lb/sec

$\eta_d = 0.85$

$\eta_{cn} = 0.95$

$\dot{m}_g = 24.96$ lb/sec

$C_l = 0.1964$ Btu/lb–°R

$L_2 = 8.0.3$ Btu/lb

$T_2 = 1998$°R

$T_7 = 1638$°R

$Q_r = 21{,}340$ Btu/sec

Substitution into Eq. (A-19) gives, $Q_{rad} = 22{,}610$ Btu/sec, an increase of 6% over $\dot{m}_g L_2$. The radiator area is about 1% larger than that calculated for $\dot{m}_g L_2$ alone. Thus, the approximation that the heat rejection is equal to $\dot{m}_g L_2$ in the condenser cycle is, therefore, justified.

NOMENCLATURE

A_{rad} prime radiator area, ft²/kwe

C_f skin friction coefficient

C_{g_a} heat capacity of component a in the gaseous phase, Btu/lb mole–°F

C_l heat capacity of the liquid phase, Btu/lbm–°F

C_{l_a} heat capacity of component a in the liquid phase, Btu/lbm–°F

C_{l_b} heat capacity of component b in the liquid phase, Btu/lbm–°F

h enthalpy, Btu/lbm

J mechanical equivalent of heat

L heat of condensation, Btu/lbm

L_a heat of condensation of component a, Btu/lbm

L_b heat of condensation of component b, Btu/lbm

$\dot{m}_c$ mass flow rate of the coolant, lbm/sec

$\dot{m}_g$ mass flow rate of the gaseous phase, lbm/sec

$\dot{m}_l$ mass flow rate of the liquid, lbm/sec

p pressure, psi

Δp_i pressure drop due to injection at the nozzle entrance, psi

Δp_h pressure drop across the condensate side of the regenerative heater, psi

Δp_r pressure drop across the reactor, psi

P_e output power, kwe

P_p pump input power, kw

Q_c heat output during cooling, kw

Q_h heat exchanger heat transfer, kw

Q_l available liquid cooling, kw

Q_{rad} radiated power, kw

R ratio of component b flow to component a flow in the two-phase nozzle

T temperature, °R

V velocity, ft/sec

W_s specific weight, lbm/kwe

β mass fraction of component b in the gas

σ Stefan-Boltzmann constant

ε emissivity

η cycle efficiency

η_{cn} coolant nozzle efficiency

NOMENCLATURE (Cont'd)

η_d diffuser efficiency

η_g generator efficiency

η_p pump efficiency

θ impingement angle

ρ_l liquid density, lbm/ft^3

ρ_{l_a} density of component a liquid, lbm/ft^3

ρ_{l_b} density of component b liquid, lbm/ft^3

ψ fraction of liquid that does not impinge on the walls of the condenser

REFERENCES

1. Elliott, D. G., "Two-Fluid Magnetohydrodynamic Cycle for Nuclear-Electric Power Conversion," *ARS Journal*, Vol. 32, No. 6, June 1962, pp. 924–928.
2. Larson, J. W., *Study of Two-Phase MHD*, Report No. APR-1020, Pratt & Whitney Aircraft Corporation, Hartford, Connecticut, June 14, 1962.
3. Brown, G. A., and Lee, K. S., "A Liquid Metal MHD Power Generation Cycle Using a Condensing Ejector," *International Symposium on Magnetohydrodynamic Electrical Power Generation*, Vol. 2, Paris, France, July 1964, pp. 929–938.
4. Prem, L. L., and Parkins, W. E., "A New Method of MHD Power Conversion Employing A Fluid Metal," *International Symposium on Magnetohydrodynamic Electrical Power Generation*, Vol. 2, Paris, France, July 1964, pp. 971–984.
5. Petrick, M., and Lee, K.-Y., *Liquid MHD Power Cycle Studies*, Report No. ANL-6954, Argonne National Laboratory, Argonne, Illinois, June 1965.
6. Craig, R. T., and Wade, W. F., *Proposed Investigation of a Two-Phase Magneto-fluid-Mechanical Energy Conversion System*, Report No. ER-5402, Thompson Ramo Wooldridge, Inc., Cleveland, Ohio, June 21, 1963.
7. Powell, J. R., Zuker, M. S., Palmer, J. P., and Becker, W. W., "Studies of a Repetitive Liquid Metal Slug MHD Generator," *Engineering Developments in Energy Conversion*, American Society of Mechanical Engineers, New York City, 1965, pp. 15–32.
8. Elliott, D. G., "Analysis of the Acceleration of Lithium in a Two-Phase Nozzle," *Proceedings of the 1963 High Temperature Liquid Metal Heat Transfer Technology Meeting*, Oak Ridge, Tenn., December 1964, pp. 353–370.

REFERENCES (Cont'd)

9. Elliott, D. G., Weinberg, E., Hays, L. G., and Cerini, D. J., *Acceleration of Liquids in Two-Phase Nozzles,* Technical Report No. TR 32-987, Jet Propulsion Laboratory, Pasadena, Calif., November 1, 1966.

10. Elliott, D. G., Cerini, D. J., O'Connor, D., and Weinberg, E., "Liquid MHD Power Conversion," *Space Programs Summary No. 37-27, Vol. IV,* Jet Propulsion Laboratory, Pasadena, California, June 30, 1964, pp. 75–83.

11. Elliott, D. G., Cerini, D. J., and Weinberg, E., "Liquid-Metal MHD Power Conversion," *Progress in Astronautics and Aeronautics,* Vol. 16, Space Power Systems Engineering, Academic Press, New York, 1966, pp. 1275–1298.

12. Elliott, D. G., "Direct Current Liquid-Metal Magnetohydrodynamic Power Generation," *AIAA Journal,* Vol. 4, No. 4, April 1966, pp. 627–633.

13. Elliott, D. G., Cerini, D. J., Hays, L. G., and Weinberg, E., "Theoretical and Experimental Investigation of Liquid-Metal MHD Power Generation," Paper No. SM-74/177, *International Symposium on Magnetohydrodynamic Electrical Power Generation,* Salzburg, Austria, July 4–8, 1966.

14. Barnes, A. H., and Cage, J. F., Jr., "Electromagnetic Pumps," *Liquid-Metals Handbook, Sodium-NaK Supplement,* Atomic Energy Commission, Department of the Navy, Washington, D. C., July 1955, pp. 288–305.

15. Miguel, J., and Brown, G., "An Analytical and Experimental Investigation of a Condensing Ejector with a Condensable Vapor," 1st AIAA Annual Meeting, Paper No. 64-469, Washington, D. C., June 29–July 2, 1964.

16. Rose, R., *Steam Jet Pump Analysis and Experiments,* Report No. WAPD-TM-227, Wright-Patterson Air Force Base, Ohio, June 1960.

17. Hays, L., *Investigation of Condensers Applicable to Space Power Systems, Part II, Jet Condensers,* Report 1588-Final, Electro-Optical Systems, Inc., Pasadena, Calif., November 1962.

18. Elliott, D., Cerini, D., Hays, L., and Weinberg, E., "Liquid MHD Power Conversion," *Space Programs Summary No. 37-37, Vol. IV,* Jet Propulsion Laboratory, Pasadena, California, February 28, 1966, pp. 118–122.

19. Elliott, D. G., Cerini, D. J., Otte, H., and Weinberg, E., "Liquid MHD Power Conversion," *Space Programs Summary No. 37-23, Vol. IV,* Jet Propulsion Laboratory, Pasadena, California, October 31, 1963, pp. 132–135.

20. Lemmon, A. W., Jr., Deem, H. W., Eldridge, E. A., Hall, E. H., Matolich, J., Jr., and Walling, J. F., *Engineering Properties of Potassium,* Final Report, Report No. Batt-4673-Final, Battelle Memorial Institute, Columbus, Ohio, December 31, 1963.

21. Ewing, C. T., Stone, J. P., Spann, J. R., Steinkuller, E. W., Williams, D. D., and Miller, R. R., *High Temperature Properties of Potassium,* Report No. NRL 6233, U. S. Naval Research Laboratory, Washington, D. C., September 24, 1965.

22. Tepper, F., Murchison, A., Zelenak, J. S., and Roehleih, F., *Thermophysical Properties of Rubidium and Cesium,* Report No. ML-TDR-64-42, MSA Research Corporation, Callery, Pennsylvania, May 1964.

23. Foote Mineral Company, Technical Data Bulletin 101, April 1959, Philadelphia, Pa.

REFERENCES (Cont'd)

24. Taylor, J. W., "The Surface Energies of the Alkali Metals," *Philosophical Magazine*, Vol. 46, 1955, pp. 867–876.

25. Tepper, F., Udavcak, R., and Zelenak, J., *Determination of the Solubility of Potassium and Cesium in Lithium*, Report No. MSAR 64-19, MSA Research Corporation, Callery, Pennsylvania, April 16, 1964.

ACKNOWLEDGMENT

The authors would like to express their appreciation to Mr. Stanley Gardner for reducing the large amount of computer output to a usable form.